

Mechanistic Aspects of the Electrocatalytic Oxygen Evolution Reaction over Ni–Co Oxides

Leila Negahdar, Feng Zeng, Stefan Palkovits, Cornelia Broicher, and Regina Palkovits*^[a]

The electrocatalytic oxygen evolution reaction (OER) presents the key transformation in electrochemical water-splitting majorly determining energy efficiency and economics of hydrogen generation. In this study, the kinetics of the OER over Ni–Co oxide structured by KIT-6 templating and non-structured Ni–Co oxide catalysts in alkaline solution have been investigated aiming for insight with regard to the respective kinetically relevant surface reactions. Steady-state Tafel plot analysis and electrochemical impedance spectroscopy (EIS) were used to determine kinetic parameters, Tafel slopes and the order of reaction. A dual Tafel slope behavior was observed for both

catalysts. Tafel slopes of ca. 40 and 120 mVdec⁻¹ and 90 and 180 mVdec⁻¹ at low and high overpotentials appear for structured and non-structured Ni–Co oxide, respectively. A reaction order of unity was observed for structured Ni–Co oxide, while non-structured Ni–Co oxide possessed a fractional reaction order in the high overpotential region. The kinetics of OER over structured Ni–Co oxide were governed by Langmuir adsorption with the rate-limiting step after primary adsorption of surface intermediates. In contrast, non-structured Ni–Co oxide obeyed the Temkin adsorption isotherm condition with the primary adsorption step being rate-limiting.

1. Introduction

Alkaline electrocatalytic oxygen evolution is an industrially and environmentally important process for the generation of hydrogen in water-splitting technologies. Hydrogen gas is believed to be an important fuel of the future due to its high gravimetric energy density and clean combustion. The efficiency of the oxygen evolution reaction (OER) is limited since the reaction takes place at high anodic overpotential.^[1,2] There has been extensive research on the development of OER electrocatalysts with the major aims of avoiding noble metal electrodes and reducing the overpotential at high current density.^[3] Amongst the most promising non-noble metal catalysts are electrodeposited Ni and Co oxides and their mixed oxides. Nickel-cobalt mixed oxides present promising OER anodic materials because of high corrosion stability, relatively low reaction overpotentials, availability and viable costs.^[4–7]

In our recent research on OER catalyst synthesis, we developed Ni–Co oxides using in-situ hydrothermal synthesis with and without the presence of mesostructured silica (KIT-6) as a template.^[8] Amongst all materials, the structured Ni–Co oxide named NiCoOS (NiCo₂O₄-KIT-6) had the highest apparent catalytic activity and good stability, whereas the unstructured nitrate derived NiCoO (Ni_{1.7}Co_{1.3}O₄) showed lower activity (Figure S4). Comprehensive electrochemical analysis revealed not

only an enhanced electrochemical surface area (ESCA) of structured Ni–Co oxide but also superior intrinsic catalyst activity (Figure S5). Accordingly, structuration influences the materials' activity beyond simply increasing the exposed electrochemical surface area. We proposed that these distinct performances were due to modified surface properties. To gain further insights into the origin of this enhanced catalytic activity, we herein present a detailed kinetic and mechanistic analysis of these structured and unstructured materials aiming for a fundamental molecular understanding of the observation differences in the surface specific materials' performance.

The central challenge of OER is to understand the mechanistic details required for efficient catalysis. The kinetics of OER are rather complicated since the metal oxide catalyses the oxygen evolution and not the metal itself.^[9–11] Therefore, the catalytic activity of the electrocatalytic system can be influenced by factors like the surface and bulk structure of the oxide film, the synthesis of the oxide and the experimental history of the electrode. Moreover, OER involves O–O bond formation that is coupled with the transfer of four electrons in a concerted multistep reaction. Therefore, OER may follow any of a number of different reaction pathways [Eq. (1)].^[12–14]



Over the past decades, several studies have been devoted to understanding the OER mechanism on Ni (oxide) catalysts in alkaline solution.^[15–18] Nonetheless, little mechanistic agreement has been achieved. Hence, a systematic study of the OER over transient metal oxides is required to elucidate the most reliable reaction mechanism. This study focusses on a systematic kinetic investigation of OER over structured and non-structured Ni–Co oxide named NiCoOS and NiCoO in the following using several techniques such as steady-state polarization and electrochemical impedance spectroscopy (EIS). Key kinetic parameters that

[a] Dr. L. Negahdar, F. Zeng, Dr. S. Palkovits, C. Broicher, Prof. Dr. R. Palkovits
Institut für Technische und Makromolekulare Chemie
RWTH Aachen University
Aachen 52074 (Germany)
E-mail: palkovits@itmc.rwth-aachen.de

Supporting information for this article is available on the WWW under
<https://doi.org/10.1002/celec.201901265>

© 2019 The Authors. Published by Wiley-VCH Verlag GmbH & Co. KGaA.
This is an open access article under the terms of the Creative Commons
Attribution License, which permits use, distribution and reproduction in any
medium, provided the original work is properly cited.

describe the electron-transfer reactions at the interface allow insight into plausible mechanisms of the OER explaining the different catalytic activities of the materials.

2. Results and Discussion

2.1. Electrochemical Impedance Spectroscopy (EIS)

Measuring electrochemical impedance spectroscopy of the reaction at controlled potentials is an important experimental route to understand the OER mechanism. A series of electrochemical impedance spectroscopy (EIS) spectra for NiCoOS and NiCoO catalysts recorded in the direction of increasing potential are presented in the Bode and in the Nyquist complex plane plots shown in Figure S1. The impedance raw data were simulated in terms of the equivalent circuit model depicted in Figure 1 known as Armstrong-Henderson equivalent circuit.^[19] In the equivalent circuit, R_s represents the uncompensated solution resistance, R_{ct} is the charge transfer resistance, and the

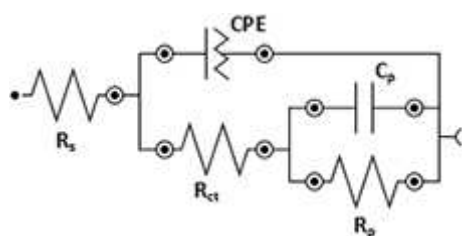


Figure 1. Equivalent circuits for fitting EIS data obtained for OER.

resistance R_p and capacitance C_p represent the parameters associated with the relaxation of the surface coverage of an adsorbed intermediate in the OER mechanism.^[20,21] When fitting the EIS data, a constant phase element, CPE, in place of pure capacitors was applied due to frequency dispersion of the capacitance at the electrode/solution interface.^[15]

The CNLS (complex non-linear least square) fitting algorithm is used to fit the raw impedance data to the equivalent circuit model depicted in Figure S2. The best fit values of the equivalent circuit elements are presented in Table S1 and S2. To have a closer look into the individual contributions of each faradaic element, we plotted the fitting values obtained in the equivalent circuit model as a function of applied potential (Figure 2). The charge transfer resistance R_{ct} is a total charge resistance for the overall rate of OER. In the theory provided by Harrington and Conway, the reciprocal resistance $1/R_{ct}$ is equal to the sum of reciprocal resistances of each charge transfer steps in OER.^[20] The variation of R_{ct} as a function of the applied potential is plotted in Figure 2(a). The resistance decreases as the potential increases for both electrodes indicating increased electron transfer kinetics, which is consistent with a Faradaic process. Figure 2(b) exhibits the double-layer capacitive behaviour of the OER process. It is clear that both electrodes show similar double-layer capacitive behaviour. The value for the double-layer capacity of NiCoOS is almost 4 times higher than NiCoO at lower potential. Such an elevated value of C_{dl} is expected to be related to the oxide covered nature of the electrode surface and is likely a reflection of the increasing concentration of charged surface states as the OER progresses.^[12]

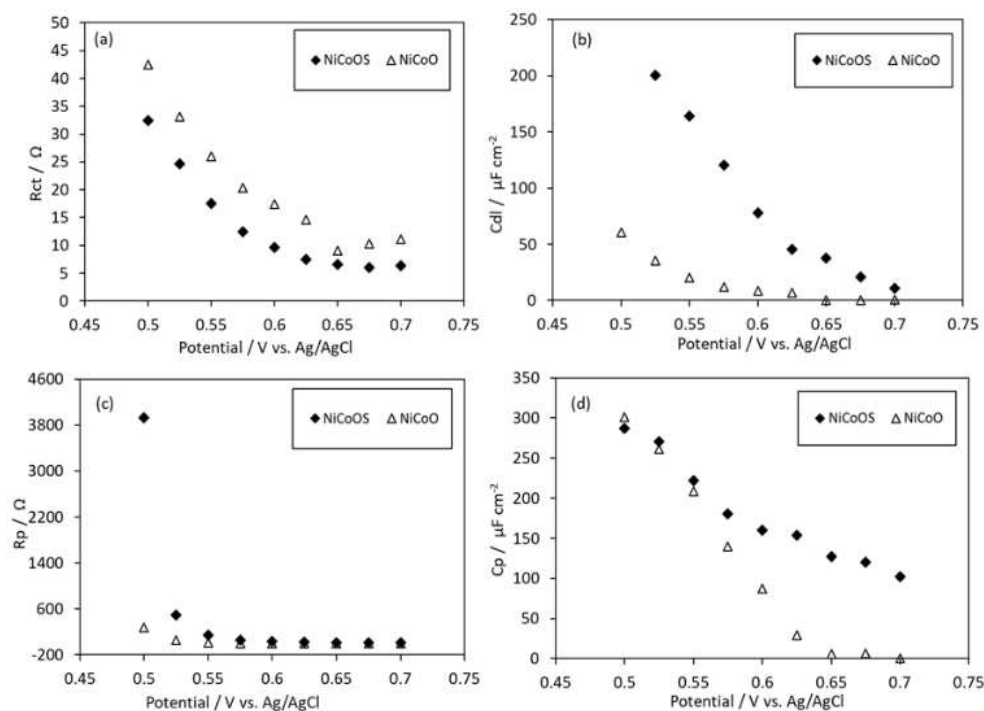


Figure 2. Fitting values plotted as a function of applied potential, (a) Charge transfer resistance (R_{ct}); (b) Double-layer capacity (C_{dl}); (c) Resistance (R_p); (d) Capacitance (C_p).

The value of C_{dl} decreases as the potential increases. This observation was reported by Bisquert et al. and the authors suggested that the decrease in capacitance at higher potentials is due to the strong gas bubble evolution which reduces the exposed surface area of the electrode.^[22,23] Figure 2 (c) and (d) illustrate the variation of R_p and C_p with potential. The C_p - R_p loop in the equivalent circuit model is associated with the surface intermediate. R_p decreases significantly with applied potential. Generally, R_p is related to the rate of surface intermediates formation. As potential increases, the intermediate species can easily be formed, consequently, R_p decreases. At potentials above 0.5 V, there is little difference in the R_p values of both electrodes. However, at low potential of 0.5 V, the resistance for NiCoOS is significantly higher. The term C_p can be related to the changing concentration of charged intermediates as the OER progresses. For NiCoO and NiCoOS, C_p decreases with potential, which is expected for a capacitance arising from a Faradic process. However, the two C_p values vary significantly from each other at higher potentials, suggesting that different charging processes and different intermediates are involved in the rate determining step (RDS) of these materials.^[12]

2.2. Tafel Analysis

Steady-state polarization techniques are the basis of Tafel analysis. The relationship between the steady-state anodic current and applied potential can be expressed in logarithmic form shown in [Eq. (2)].^[24]

$$\log(i) = \frac{\eta}{b} + \log(i_0) \quad (2)$$

However, the identification of the true mechanistic significance of Tafel slopes will be best achieved when several experimental techniques are combined. EIS techniques also with following expression [Eq. (3)] can be used to generate the Tafel plot.^[25,26]

$$\log\left(\frac{1}{R_f}\right) = \frac{\eta}{b} + \log\left(2.303 \frac{i_0}{b}\right) \quad (3)$$

In the above equations, R_f is the Faradaic resistance which is calculated from the fitting parameters as $(R_{ct} + R_p)$, η is the overpotential (E vs. RHE - 1.23), i_0 is the exchange current density and b is the Tafel slope. By implying the inverse slope of a plot of $\log(i)$ or $\log\left(\frac{1}{R_f}\right)$ against η the Tafel slope (b) can be determined. A comparison of the steady-state polarization and EIS Tafel plots is presented in Figure 3. The presence of two distinct linear regions is an observable feature of the OER.^[27] Tafel slopes of ca. 40 mV dec⁻¹ and ca. 90 mV dec⁻¹ in the low overpotential region and ca. 120 mV dec⁻¹ and ca. 180 mV dec⁻¹ in the higher overpotential region have been observed for NiCoOS and NiCoO, respectively. These changes in the Tafel slope with increasing potential are mostly attributed to a change in the rate determining step or the influence of

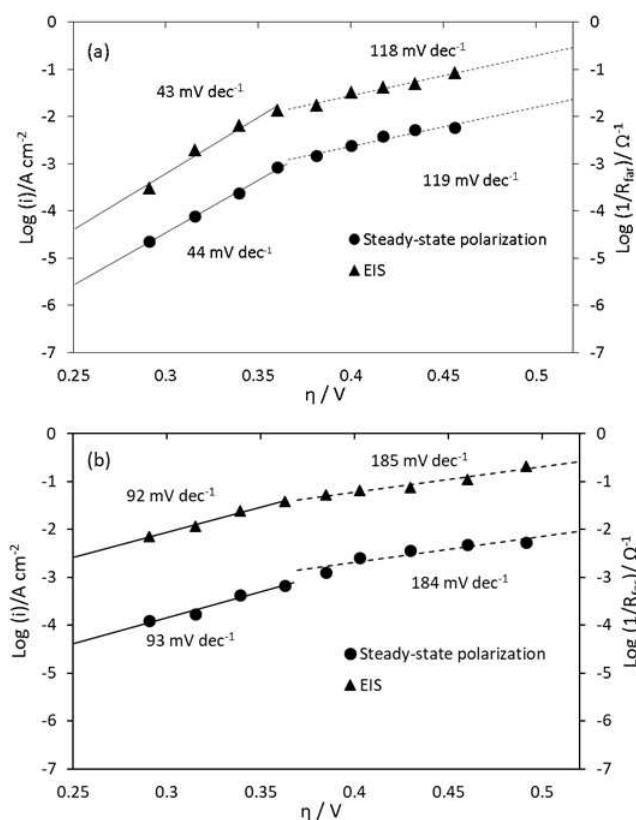


Figure 3. Comparison of the Tafel plots generated using EIS and Steady-state polarization data; (a) NiCoOS, (b) NiCoO.

potential variation on the adsorption of reaction intermediates.^[28,29]

From an experimental point of view, increases in the Tafel slope with applied potential could be the consequence of a reduction in the effective electrode surface area with increasing gas evolution at the higher applied potentials. Moreover, mass transfer limitations at higher overpotential can result in an increase in Tafel slope. However, the agreement between two different methods indicates that the dual Tafel behavior is not an artefact but is rather mechanistically significant.^[25,26]

The elucidation of Tafel slopes can provide the basis to differentiate between possible reaction mechanisms. The larger Tafel slope indicates greater polarization with increasing current density and the lower Tafel slope indicates an efficient electrocatalytic performance.^[30,31] The Tafel slope is a composite parameter providing information on the stoichiometry and succession of steps in the overall reaction and can be defined by the transfer coefficient α_a [Eq. (4)]:^[29,32,33]

$$\alpha_a = \frac{1}{b} \left(\frac{2.303RT}{F} \right) \quad (4)$$

From equation (4), it is observable that the Tafel slope and the charge transfer coefficient exhibit an inverse relationship which means if the Tafel slope of an OER is low, the activity will be high and vice-versa. The transfer coefficient is experimentally quantifiable and commonly applied in the kinetic analysis of

electrode processes. It can be described by the following equation:^[13,32,34]

$$\alpha_a = n_f/\nu + n_r\beta \quad (5)$$

Where, n_f is the number of electrons transferred before the RDS, ν is the stoichiometric number with a typical value of one, n_r is the number of electrons transferred in each occurrence of the RDS, and β is the symmetrical potential energy barrier factor also known as electrochemical Brønsted factor with a value of 0.5–1.^[33,35,36]

However, Eq. (5) provides more mechanistic information. If in an OER process, the rate determining step is a step subsequent to the first electron transfer step and $\beta = 0.5$ then, $n_r = 1$ and $n_f = 1$, thus $\alpha_a = 1.5$ predicting the Tafel slope of ca. 40 mVdec⁻¹ in the low overpotential region. With the same rate determining step, if the RDS is a chemical step ($n_r = 0$) and preceded by a one electron transfer step occurring twice ($\nu = 2$) and in any single step one electron is transferred ($n_f = 1$) then $\alpha_a = 0.5$ implying a Tafel slope of ca. 120 mVdec⁻¹ in the high overpotential region for NiCoOS.^[30,33,34]

Nonetheless, in case of NiCoO with Tafel slopes of ca. 90 and 180 mVdec⁻¹, it is difficult to interpret the mechanism from the transfer coefficient unless the symmetrical potential energy barrier factor (β) would have different values of generally accepted 0.5. We will further discuss this point in the electrochemical kinetics section.

2.3. Electrochemical Reaction Order

Determination of the reaction order is an important part of reaction kinetics. In electrocatalytic reactions, the reaction orders depend on the isotherm adsorption of the reactants at the electrode interface and the adsorption of reaction intermediates.^[30] Theoretically, the reaction order provides the relationship between the reaction rate and the concentration of the reactants, which is key in mechanistic interpretations. The electrochemical reaction order m_x can be expressed as:^[37]

$$m_{x, \nu} = \left(\frac{\partial \log i}{\partial \log a_x} \right)_{\nu} \quad (6)$$

Where, a_x is the activity of mechanistically significant reactant x , and V denotes the applied potential.

Reaction order plots were generated at a range of potentials for our system with dual Tafel behavior. Distinct reaction orders can be associated with each Tafel region. Reaction order plots with respect to OH⁻ ion activity constructed from pH dependent *iR* corrected steady-state polarization curves are presented in Figures 4 (a) and (b).

A reaction order of ca. 1 was obtained at potentials located in the high and low overpotential regions respectively for NiCoOS (Figure 5 (a)). In case of NiCoO, the order of reaction is about 1.5 and 0.8 in the high and low Tafel regions, respectively (Figure 5 (b)). A change in reaction orders arises when changes

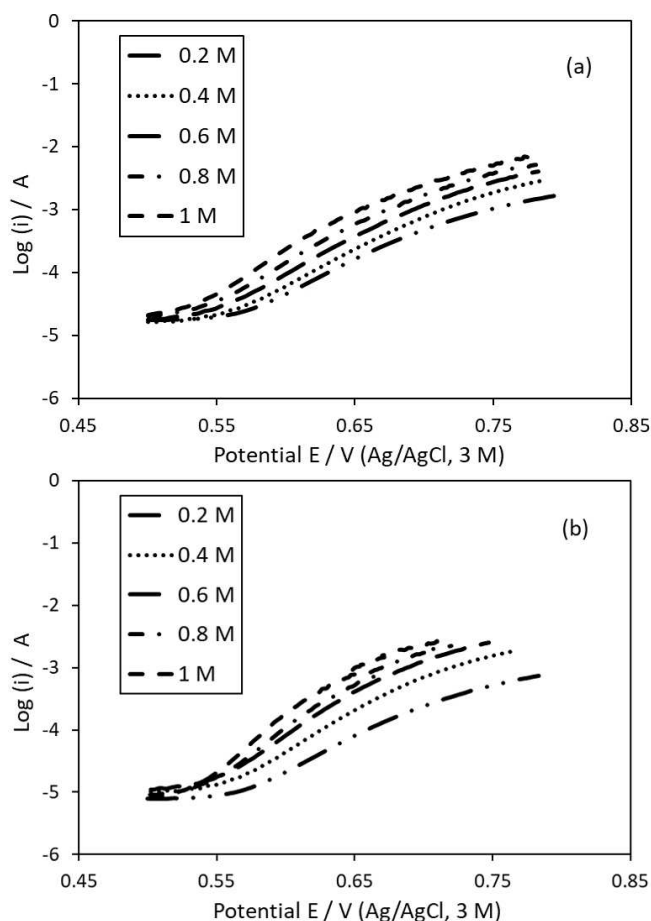


Figure 4. *iR* corrected steady-state polarization curves at various pH solutions; (a) NiCoOS (b) NiCoO.

of adsorption conditions occur corresponding to changes of the degree of coverage by intermediates.

A reaction order of one suggests that only one hydroxide ion reacts at each active site for all steps including the RDS and it may be rationalized by Temkin or Langmuir adsorption conditions.^[30,38,39] Similarly, if the order of reaction is two, then a total of two OH⁻ equivalents can be assumed to be involved in the overall reaction prior to and including the RDS.^[27] However, rationalizing fractional reaction orders is more challenging and potentially suggests the presence of competing pathways. Accordingly, the overall reaction order depends on the fraction of catalytically active sites promoting each of the individual pathways. Fractional reaction orders can also occur depending on the relative coverage of the reaction intermediates. A fractional reaction order of $m_{OH^-} = 1.5$ was observed by Bockris and Lyons for a range of cobalt perovskites and for aged passive iron oxides. In both cases the fractional reaction orders was rationalized by Temkin adsorption rather than Langmuir.^[13,38]

In general, the coverage by intermediates in Langmuir isotherm adsorption is assumed in either approaches to zero or unity ($\theta \rightarrow 0$ or $\rightarrow 1$) with the heat of adsorption being negligible. But in case of fractional coverage ($0.2 < \theta < 0.8$); the heat of adsorption is assumed to change linearly with coverage which

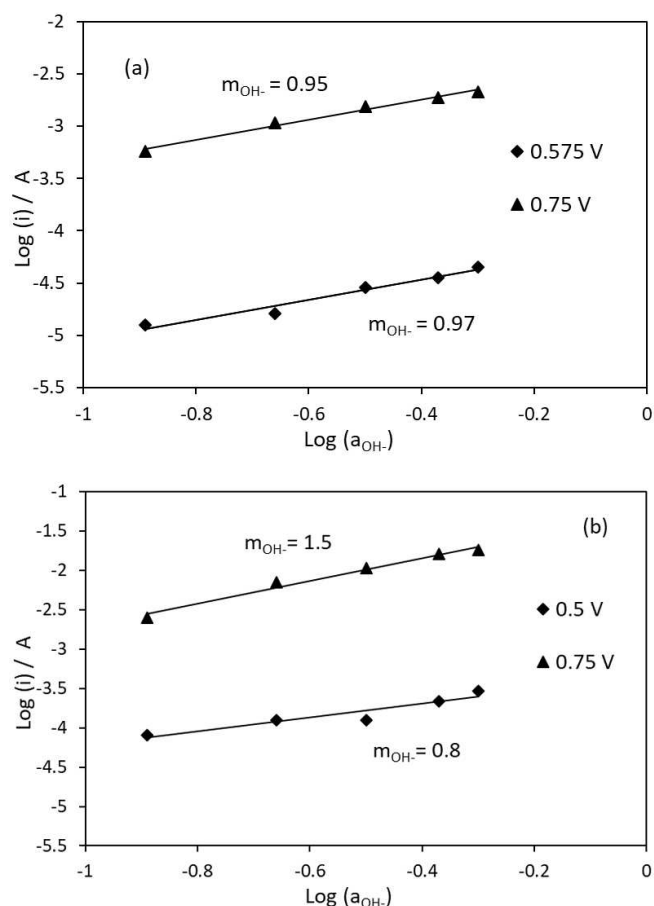


Figure 5. Reaction order plot based on polarization curves; (a) NiCoOS (b) NiCoO.

implies Temkin conditions.^[13] The Temkin isotherm condition is based on the decrease in the free energy of adsorption of an intermediate species with increasing total coverage resulting in an increase in the free energy of activation for that step and vice versa. The Temkin isotherm condition is more applicable when two or more adsorbed intermediate species are present simultaneously on an electrode surface leading to the fractional reaction order.^[48–50]

2.4. Electrochemical Kinetic Analysis

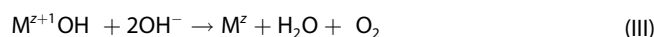
Before deriving the reaction rate equations, we verified the absence of mass transfer limitations. The effect of mass transfer of the evolved oxygen from the surface to the solution was examined using the rotating disk method. Figure S3 illustrates the dependence of currents at constant voltage on the rotation speed. The current changes slightly (5%) with increasing rotation speed. Hence, the effect of mass transfer of the evolved oxygen is negligible.^[40,41]

2.5. Mechanism of OER

In principle, electrocatalytic reactions follow two mechanistic types: (1) reactions will proceed by electron transfer to or from a molecule or ion, producing a chemisorbed species on the electrode surface and with further steps, will form a stable molecule through a heterogeneous chemical recombination step; (2) reactions which involve an initial dissociative or associative, chemisorption step followed by electrochemical charge-transfer steps involving the initially formed chemisorbed intermediates.⁴²

Over the past years, several possible mechanisms for OER have been proposed with notable studies of Brockris, Krasil'shchikov, Conway and Lyons.^[10,13,15,17,29] Most of the proposed mechanisms followed the type (1) which starts by adsorption of the hydroxide ions on the catalyst active site. Subsequently, the reaction proceeds with formation of a range of surface adsorbed intermediates which could then react with each other via various disproportionation or bimolecular decomposition reactions or undergo nucleophilic attack to release oxygen as O₂.^[43,44]

However, in order to derive a rate expression for OER, it is necessary to describe the overall reaction as a sequence of elementary one electron transfer steps. In this way, the overall rate of OER can be expressed in terms of the slowest step or RDS. Depending on which step is rate determining, the reaction sequences lead to different Tafel slope and reaction orders. To explain the mechanism of NiCoOS, we followed the proposed OER pathways by O'Grady's as outlined below:^[31]



Where, M^z is a transition-metal ion with valence state z.

Based on Butler-Volmer kinetics, applying the quasi-equilibrium method and assuming that all steps are in equilibrium except the rate-determining; the rates of reaction for step (I) in forward and reverse direction can be written as [Eqs. (7)–(8)].^[35,45]

$$f_1 = k_1^0 a_{OH^-} (1 - \theta) \exp\left[\frac{\beta F \eta}{RT}\right] \quad (7)$$

$$f_{-1} = k_{-1}^0 \theta \exp\left[-\frac{(1 - \beta) F \eta}{RT}\right] \quad (8)$$

Where, *f* is flux with units of mole cm⁻² s⁻¹, *θ* is the surface coverage, *k_i⁰* is standard electrochemical rate constant. Under pseudo-equilibrium and low coverage, the surface coverage will be $\theta = K a_{OH^-} \exp\left[\frac{F \eta}{RT}\right]$. If we assume the second step is rate determining, then the net reaction flux can be written as [Eq. (9)]:

$$f_T = f_2 = Kk_2^0 a_{OH} \exp\left[\frac{(1+\beta)F\eta}{RT}\right] \quad (9)$$

Assuming a symmetrical electron transfer energy barrier for the second step is $\beta = 0.5$, we can derive the Tafel slope and order of reaction from the following equations [Eqs. (10)–(11)]:

$$b = \left(\frac{\partial \eta}{\partial \ln f_T}\right)_{a_{OH}} = 2.303 \frac{RT}{(1+\beta)F} = 2.303 \frac{2RT}{3F} \quad (10)$$

$$m_{OH^-} = \left(\frac{\partial \ln f_T}{\partial \ln a_{OH}}\right)_\eta = 1 \quad (11)$$

Hence, it is clear that the proposed mechanism predicts the experimental kinetic parameters of Tafel slope of $\sim 40 \text{ mV dec}^{-1}$ and reaction order of unity at lower overpotentials for NiCoOS.

The experimentally observed Tafel slope of $2.303 \left(\frac{2RT}{F}\right) \sim 120 \text{ mV dec}^{-1}$ can be ascribed to the change of adsorbed species surface coverage at high potential when $\theta \rightarrow 1$ under Langmuir adsorption conditions (S1, S-12 to S-14). Accordingly, the coverage θ changes from low coverage to high coverage with increasing potential, which is characterized by the change in Tafel slope from 40 mV dec^{-1} to 120 mV dec^{-1} .

Considering the non-integral reaction orders of NiCoO, we opt for Temkin adsorption isotherm conditions assuming the fractional coverage of the reaction intermediates. Following the same mechanism proposed by O'Grady's and assuming the first electron transfer step to be in quasi-equilibrium, the rates of reaction for step (I) in forward and reverse direction can be written as [Eqs. (12)–(13)]:^[31]

$$f_1 = k_1^0 a_{OH} (1 - \theta) \exp\left[\frac{\beta F \eta}{RT}\right] \exp\left[\frac{-\gamma g \theta_T}{RT}\right] \quad (12)$$

$$f_{-1} = k_{-1}^0 \theta \exp\left[-\frac{(1-\beta)F\eta}{RT}\right] \exp\left[\frac{(1-\gamma)g\theta_T}{RT}\right] \quad (13)$$

Where, g is the rate of change of the free energy of adsorption and, γ is symmetry factor ($0 < \gamma < 1$). If we assume the first step as rate-determining for low overpotential region, then the net reaction flux can be written as [Eq. (14)]:

$$f_T = f_1 = k_1^0 a_{OH} (1 - \theta) \exp\left[\frac{\beta F \eta}{RT}\right] \exp\left[\frac{-\gamma g \theta_T}{RT}\right] \quad (14)$$

With further substitution of $g\theta_T$ in eq. (S-19) into Eq. (15), we have:

$$f_T = k_1^0 a_{OH}^{1-\gamma} (1 - \theta) K^{-\gamma} \exp\left[\frac{(\beta - \gamma)F\eta}{RT}\right] \quad (15)$$

Now, we can derive the Tafel slope and the order of reaction from following equations [Eqs. (16)–(17)]:

$$b = \left(\frac{\partial \eta}{\partial \ln f_T}\right)_{a_{OH}} = 2.303 \frac{RT}{(\beta - \gamma)F} \quad (16)$$

$$m_{OH^-} = \left(\frac{\partial \ln f_T}{\partial \ln a_{OH}}\right)_\eta = 1 - \gamma \quad (17)$$

For NiCoO, the experimental kinetic analysis predicted a Tafel slope of $2.303 \left(\frac{3RT}{2F}\right) \sim 90 \text{ mV dec}^{-1}$ for low overpotentials. With the reaction order of ca. 0.8, we can anticipate the value of γ to be about 0.25. Thus, with value of $\beta = 1$ the Tafel slope of $\sim 90 \text{ mV dec}^{-1}$ in the low overpotential region can be admitted. On the other hand, if following an O'Grady's path, the third step is assumed to be rate-determining, then the net reaction flux can be written as [Eq. (18)]:^[31]

$$f_T = f_3 = k_3^0 a_{OH}^2 (K a_{OH})^{(1-\gamma)} \theta \exp\left[\frac{(\beta - \gamma + 1)F\eta}{RT}\right] \quad (18)$$

Now, we can derive the Tafel slope and the order of reaction from following equations [Eqs. (19)–(20)]:

$$b = \left(\frac{\partial \eta}{\partial \ln f_T}\right)_{a_{OH}} = 2.303 \frac{RT}{(\beta - \gamma + 1)F} \quad (19)$$

$$m_{OH^-} = \left(\frac{\partial \ln f_T}{\partial \ln a_{OH}}\right)_\eta = 2 - 2\gamma \quad (20)$$

The experimental value of the reaction order of $m_{OH^-} = 1.5$ in the high overpotential region estimates $\gamma = 0.25$ and $\beta = 0.5$ which predicts a Tafel slope of $\sim 180 \text{ mV dec}^{-1}$ in the high overpotential region.

However, it seems the symmetry factor β has a major impact on kinetics of NiCoO. The meaning of the symmetry factor β has been interpreted based on different models in the literature. Based on Butler, β is the fraction of the potential distance profile across the electrical double layer that enhances the electron transfer rate by bringing the reactant on top of the potential-energy barrier, where the transition state complex is located. If the potential energy barrier is symmetric meaning it is symmetrically located within the electrical double layer, the value of β equals 0.5; otherwise, it is asymmetric and β possesses different values.^[52] On the other hand, in Marcus theory, β is regarded as a multicomponent term that depends upon reorganization of the solvent in the transition state and is a function of the applied overpotential. This theory predicts a β value very close to 0.5 and a large deviation can occur in case of asymmetric situations.^[53] Large deviations of β from the 0.5 value are also expected if the reactant exchanges an electron with the metal while being in the adsorbed state.^[54]

Based on these kinetic analyses, Tafel slope and order of reaction are two key aspects depicting the differences in intrinsic catalytic activities. NiCoOS possessed a lower Tafel slope, which is essential for efficient electrocatalytic activity. This low Tafel slope is most probably associated with the second reaction step being rate-determining. The low Tafel slope also indicates a strong adsorption of surface intermedi-

ates in the primary step hampering the following step which becomes rate limiting. On the other hand, in case of NiCoO the primary step is proposed to be rate limiting according to the only weak adsorption of the surface intermediate at the initial stage.

The origin of such differences in surface adsorption energies and the resulting coverage at constant potential is currently still difficult to rationalize in form of a molecular surface mechanism. Nevertheless, structuring of NiCoOS is suggested to result in either a different exposure of certain surface facets or a certain degree of surface roughness impacting these properties (S8 and S9). Without doubt, further studies are required to tackle the challenge of a proper translation of such kinetic analyses into comprehensive insight into the surface mechanism.

3. Conclusions

In conclusion, we have studied the kinetics of OER over structured and non-structured Ni–Co oxide catalysts namely, NiCoOs and NiCoO. Steady-state polarization, EIS and order of reaction methods showed to complement each other in kinetic analysis. A dual Tafel slope behavior was observed. A mechanism has been developed based on O'Grady's path. The analyses suggested different reaction pathways as rate-limiting step for both electrodes. The Tafel slope and order of reaction obtained from the proposed mechanism showed to be consistent with those from experimental kinetic analysis. The differences in catalytic activity were explained based on several factors including Tafel slope, reaction order and potential energy barrier. Differences in the strength of adsorption of surface intermediates shift the rate limiting step. In case of NiCoO weak adsorption causes the primary step to be rate limiting, while stronger adsorption in case of NiCoOS suggests the subsequent surface step to be rate limiting.

Experimental Section

The catalysts NiCoOS (NiCo₂O₄-KIT-6) and NiCoO (Ni_{1.7}Co_{1.3}O₄) were synthesized as reported previously.⁸ The electrochemical measurements were carried out on an Autolab PGSTAT 302 N electrochemical workstation connected to a three-electrode cell. A glassy carbon rotating disc electrode (RDE) (4 mm diameter), an Ag/AgCl electrode filled with 3 M KCl solution, and a glassy carbon rod were used as the working electrode, the reference electrode, and the counter electrode, respectively. The working electrode was modified with a catalyst ink suspension to obtain a catalyst loading of 0.16 mg cm⁻².

Catalyst inks were prepared by dispersing 2 mg catalyst in 500 μL Nafion solution containing 45.5 v% H₂O, 45.5 v% ethanol, and 9.0 v% Nafion. The ink was shaken and sonicated for 15 min. 5 μL of catalyst ink was pipetted onto the pre-cleaned glassy carbon rotating disk electrode (RDE) surface with a geometric area of 0.126 cm², to form a catalyst film with a loading of 160 μg cm⁻². The electrodes were polished using 3 μm and 1 μm polishing paper and 1 μm and 0.05 μm polishing paste, sonicated and raised in ethanol and milli-Q water before use. After the polymer film was deposited on the glassy carbon electrodes, it was dried at room temperature for 30 min.

The electrocatalytic activity was investigated by cyclic voltammetry using a potentiostat (Metrohm) @ 0.005 V/s, 2500 rpm. Potentials were referenced to the reversible hydrogen electrode (RHE). Before recording any data, the catalysts were first subjected to continuous potential cycling (CV) until steady voltammograms were obtained (100 CVs @ 0.1 V/s).

The polarization characteristics of the OER were tested in the potential region from 0.0 V to 0.7–0.8 V by sweeping the potential with 5 mVs⁻¹. Electrochemical impedance spectroscopy (EIS) has been measured in the frequency range from 100 kHz to 0.05 Hz, at the amplitude of 5 mV RMS and potentials from 0.5 to 0.7 V vs Ag/AgCl with the step of 0.025 V. The real and imaginary components of electrochemical impedance spectra in the Nyquist plot were analysed using the fitting program of ZView to simulate the equivalent resistances and capacitances.

Acknowledgements

We acknowledge the Federal Ministry of Education and Research (BMBF) for funding part of this work with the MANGAN research cluster BMBF-PTJ FKz 03SF0508. Feng Zeng acknowledges the China Scholarship Council for financial support.

Conflict of Interest

The authors declare no conflict of interest.

Keywords: oxygen evolution reaction · nickel-cobalt oxide · electrokinetic study · reaction mechanism · impedance spectroscopy

- [1] I. Katsounaros, S. Cherevko, A. R. Zeradjanin, K. J. J. Mayrhofer, *Angew. Chem. Int. Ed.* **2014**, *53*, 102–121; *Angew. Chem.* **2014**, *126*, 104–124.
- [2] N. T. Suen, S. F. Hung, Q. Quan, N. Zhang, Y. J. Xu, H. M. Chen, *Chem. Soc. Rev.* **2017**, *46*, 337–365.
- [3] I. Roger, M. A. Shipman, M. D. Symes, *Nat. Rev. Chem.* **2017**, *1*, 1–13.
- [4] J. Suntivich, K. J. May, H. A. Gasteiger, J. B. Goodenough, Y. Shao-Horn, *Science* **2011**, *334*, 1383–1385.
- [5] A. Eftekhari, *Mater. Today* **2017**, *5*, 37–57.
- [6] C. Zhu, D. Wen, S. Leubner, M. Oschatz, W. Liu, M. Holzschuh, F. Simon, S. Kaskel, A. Eychmüller, *Chem. Commun.* **2015**, *51*, 7851–7854.
- [7] J. Chi, H. Yu, G. Li, L. Fu, J. Jia, X. Gao, B. Yi, Z. Shao, *RSC Adv.* **2016**, *6*, 90397–90400.
- [8] C. Broicher, F. Zeng, J. Artz, H. Hartmann, A. Besmehn, S. Palkovits, R. Palkovits, *ChemCatChem* **2018**, *10*, 1–6.
- [9] D. K. Bediako, Y. Surendranath, D. G. Nocera, *J. Am. Chem. Soc.* **2013**, *135*, 3662–3674.
- [10] B. E. Conway, *Prog. Surf. Sci.* **1995**, *49*, 331–425.
- [11] J. Rossmeisl, A. Logadottir, J. K. Nørskov, *Chem. Phys.* **2005**, *319*, 178–184.
- [12] R. L. Doyle, M. E. G. Lyons, *Phys. Chem. Chem. Phys.* **2013**, *15*, 5224–5237.
- [13] J. O. M. Bockris, T. Otagawa, *J. Phys. Chem.* **1983**, *87*, 2960–2971.
- [14] A. G. C. Kobussen, G. H. J. Broers, *J. Electroanal. Chem.* **1981**, *126*, 221–240.
- [15] M. E. G. Lyons, M. P. Brandon, *Int. J. Electrochem. Sci.* **2008**, *3*, 1425–1462.
- [16] B. M. Jović, U. Lačnjevac, V. D. Jović, N. V. Krstajić, *J. Electroanal. Chem.* **2015**, *754*, 100–108.
- [17] B. E. Conway, P. L. Bourgault, *Can. J. Chem.* **1962**, *40*, 1690–1707.
- [18] X. Wang, H. Luo, H. Yang, P. J. Sebastian, S. A. Gamboa, *Int. J. Hydrogen Energy* **2004**, *29*, 967–972.
- [19] R. D. Armstrong, M. Henderson, *J. Electroanal. Chem.* **1972**, *39*, 81–90.
- [20] D. A. Harrington, B. E. Conway, *Electrochim. Acta* **1987**, *32*, 1703–1712.

- [21] B. E. Conway, E. Gileadi, *Trans. Faraday Soc.* **1962**, *58*, 2493–2509.
- [22] R. K. Shervedani, *J. Electrochem. Soc.* **1997**, *144*, 511.
- [23] A. J. Terezo, J. Bisquert, E. C. Pereira, G. Garcia-Belmonte, *J. Electroanal. Chem.* **2001**, *508*, 59–69.
- [24] J. Tafel, *Z. Phys. Chem.* **1905**, *50*, 6661.
- [25] R. L. Doyle, M. E. G. Lyons, *Phys. Chem. Chem. Phys.* **2013**, *15*, 5224–5237.
- [26] R. L. Doyle, M. E. G. Lyons, *J. Electrochem. Soc.* **2013**, *160*, 142–154.
- [27] S. Giménez, J. Bisquert, Springer, **2016**.
- [28] A. Damjanovic, M. A. Genshaw, J. O. Bockris, *J. Electrochem. Soc.* **1967**, *14*, 1107–1112.
- [29] A. Damjanovic, A. Dey, J. O. M. Bockris, *Electrochim. Acta* **1966**, *11*, 791–814.
- [30] S. B. Adler, *J. Electrochem. Soc.* **1996**, *143*, 11.
- [31] M. Lyons, *Int. J. Electrochem. Sci.* **2008**, *3*, 1463–1503.
- [32] R. Parsons, *Trans. Faraday Soc.* **1951**, *7*, 1332–1344.
- [33] R. Guidelli, R. G. Compton, J. M. Feliu, E. Gileadi, J. Lipkowski, W. Schmickler, S. Trasatti, *Pure Appl. Chem.* **2014**, *86*, 245–258.
- [34] A. Damjanovic, A. Dey, J. O. M. Bockris, *Electrochim. Acta* **1966**, *11*, 791–814.
- [35] B. E. Conway, Springer, **1999**.
- [36] J. W. Schultze, F. D. Koppitz, *Electrochim. Acta* **1976**, *21*, 327–384.
- [37] B. E. Conway, M. Salomon, *Electrochim. Acta* **1964**, *9*, 1599–1615.
- [38] M. E. G. Lyons, R. L. Doyle, M. P. Brandon, *Phys. Chem. Chem. Phys.* **2011**, *13*, 21530–21551.
- [39] R. L. Doyle, M. E. G. Lyons, *J. Electrochem. Soc.* **2013**, *160*, H142–H154.
- [40] H. Kita, S. Ye, Y. Gao, *J. Electroanal. Chem.* **1992**, *334*, 351–357.
- [41] H. Wendt, S. Rausch, T. Borucinski, *Adv. Catal.* **1994**, *40*, 87–176.
- [42] B. E. Conway, *J. Mol. Catal.* **1989**, *54*, 353–369.
- [43] H. Dau, C. Limberg, T. Reier, M. Risch, S. Roggan, P. Strasser, *ChemCatChem* **2010**, *2*, 724–761.
- [44] S. Marini, P. Salvi, P. Nelli, R. Pesenti, M. Villa, M. Berrettoni, G. Zangari, Y. Kirov, *Electrochim. Acta* **2012**, *82*, 384–391.
- [45] S. Schuldiner, *J. Am. Chem. Soc.* **1966**, *43*, 470.
- [46] R. Parsons, *Trans. Faraday Soc.* **1958**, *54*, 1053–1063.
- [47] W. O'Grady, C. Iwakura, J. Huang, E. Yeager, *Proceedings of the symposium on electrocatalysis*, **1974**, 286–301.
- [48] M. I. Temkin, *Zh. Fiz. Khim.* **1941**, *15*, 296.
- [49] B. E. Conway, E. Gileadi, *Trans. Faraday Soc.* **1962**, *58*, 2493.
- [50] M. E. G. Lyons, W. Breen, J. F. Cassidy, *J. Chem. Soc. Faraday Trans.* **1991**, *87*, 115.
- [51] K. J. Vetter, Academic Press, New York, **1967**.
- [52] A. V. Butler, *Trans. Faraday Soc.* **1924**, *19*, 729.
- [53] R. A. Marcus, *Can. J. Chem.* **1959**, *37*, 155.
- [54] E. Gileadi, *J. Electroanal. Chem.* **2011**, *660*, 247.

Manuscript received: July 31, 2019
 Revised manuscript received: October 8, 2019
 Accepted manuscript online: October 9, 2019